https://doi.org/10.37434/tpwj2022.03.03

FOR DISCUSSION

INFLUENCE OF WELDING MODES ON DECARBURIZATION IN THE HEAT-AFFECTED ZONE OF R91 STEEL IN WELDED JOINTS OF DISSIMILAR STEELS AFTER HIGH-TEMPERATURE TEMPERING

M.O. Nimko, V.Yu. Skulskyi, A.R. Gavryk, I.G. Osypenko

E.O. Paton Electric Welding Institute of the NASU
11 Kazymyr Malevych Str., 03150, Kyiv, Ukraine

ABSTRACT

Carbon migration from the lower-alloyed to the higher-alloyed steel takes place in welded joints of dissimilar steels, as a result of difference in carbon chemical potential after tempering and in high-temperature service. Decarburization in the HAZ near-weld zone of the lower-alloyed steel can lead to formation of service defects and subsequent failure. From mass transfer theory it is known that in polycrystalline bodies the diffusion of interstitial elements, including carbon, occurs most rapidly along the grain boundaries. Theoretically, reduction of carbon diffusion can be achieved by increasing the grain dimensions in the HAZ near-weld zone that will lead to reduction of the overall grain boundary area per a unit of volume in this zone. This work is a study of the influence of the angle of electrode inclination and welding current at deposition of austenitic metal on R91 steel on the width of the decarburized interlayer, forming at subsequent tempering at the temperatures of 700 and 760 °C. It is shown that the resultant decarburized interlayer becomes narrower with increase of the angle of electrode inclination and deposition current.

KEYWORDS: carbon diffusion, dissimilar steel joint, HAZ, decarburized interlayer, grain boundaries

INTRODUCTION

Problems related to carbon migration from the lower-alloyed steel to the higher-alloyed one started arising from the beginning of application of combined joints with austenitic stainless steels and respective welding consumables in pipe systems of boilers in 1940s. First accidents were recorded in 1950s and efforts were made to improve the equipment operation mode and to understand the causes for this phenomenon. In 1960s there was an increase in application of transition joints from austenitic materials for the needs of boiler construction, particularly when the steam temperature rose up to 566 °C. In 1970s and 1980s the scope of application and number of failures of the transition welds increased. Numerous studies of the causes for these accidents showed that carbon migration in welded joints of dissimilar steels at higher temperatures is an important factor [1].

As ferritic steels have higher carbon content than austenitic ones, the gradient of carbon concentration in the zone of contact of these steels decreases from ferritic towards austenitic steel. At higher temperatures carbon diffuses in the direction of reduction of the chemical potential gradient. It is important to note that chromium lowers the carbon chemical potential [2], while carbon content increases from ferritic-martensitic to austenitic steel. Therefore, the gradients of chromium and carbon concentration create a rather abrupt gradient of chemical potential across the fusion zone. More over, the coefficient of carbon diffusion in ferrite is much higher, than that in austenite, while the solubility is lower. These factors result in a strong driving force for carbon diffusion from ferritic to austenitic steel, leading to formation of a decarburized interlayer.

The decarburized interlayer has lower mechanical properties, which can be characterized by hardness reduction and high concentration of localized strain measured during tensile testing [1]. An important aspect of degradation of the properties associated with decarburization, is the loss of long-term hardening mechanism, because of dissolution of $M_{23}C_6$, M_7C_3 carbides and MX carbonitrides [3] that decreases the dispersion hardening. The recrystallization process also eliminates the combined influence of dislocation and subgrain-boundary hardening [4]. The consequence is the possibility of fracture inside the decarburized interlayer [1, 5, 6].

In its turn, a carburized interlayer forms in the higher-alloyed steel. In work [7], it was shown that microcracks can initiate in such a carburized interlayer. Microcracks predominantly initiate in the transition zone and are intragranular.

This necessitates reducing the decarburized interlayer in dissimilar steel joints in high-temperature service under creep conditions. It is general practice to

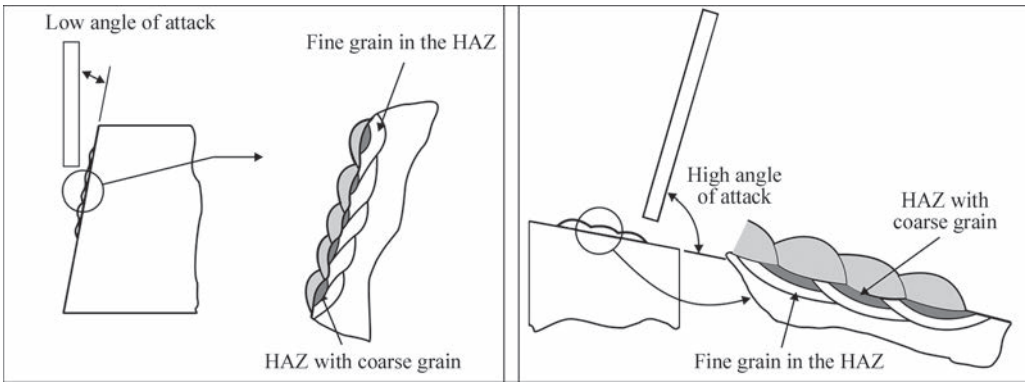

Figure 1. Technique of cladding the plate edges by austenitic metal [13]

use nickel welding consumables to reduce carbon diffusion. However, most of the researchers believe that the traditional nickel-based materials (for instance, Ni 6082, Ni 6182, Ni 6117, Ni 6625 to DSTU ISO 14172) cannot effectively completely contain carbon diffusion from martensitic steel into the weld, as most of the nickel alloys used as welding consumable, contain a large quantity of carbide formers, in particular chromium [8–11].

The problem of containment diffusion-induced carbon redistribution remains urgent and requires other approaches (methods) to solve it. In the first part of the work [12] investigations were performed of the influence of the modes of surfacing (heat input and heating temperature) by an austenitic welding consumable on development of the width of decarburized interlayer in X10CrMoVNb9-1 (R91) steel at tempering at 750 °C temperature for 7 and 18 h, and it was clarified that the interlayer width after tempering decreases with heat input increase; with increase of heating temperature from 20 to 195 °C the width of the interlayer after tempering also decreases, and then starts increasing with heating up to 300 °C. Considering that the above investigations were performed using single-interlayer austenitic deposits on martensitic steel surface, it was necessary to check the obtained regularities on real combined joints.

The objective of the study was to verify the influence of the welding mode and technique (electrode inclination angle) on decarburization kinetics in the HAZ near-weld zone of the lower-alloyed steel in the combined welded joints after high-temperature tempering.

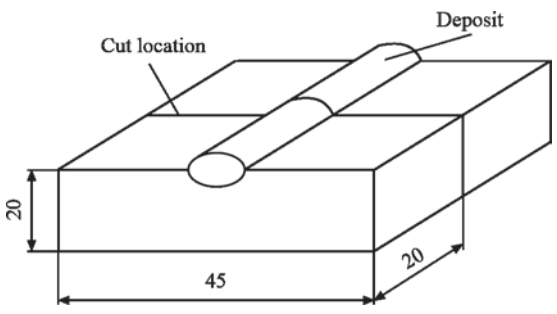

Figure 2. Scheme of cutting up the deposit into templates

INVESTIGATION PROCEDURE

Martensitic steel R91 (X10CrWMoVNb9-2 (1.4901) to DSTU EN 10216-2:2016), containing 9 % Cr (wt.%: 0.1 C; 0.34 Si; 0.47 Mn; 8.52 Cr; 0.28 Ni; 0.93 Mo; 0.2 V; 0.072 Nb; 0.06 N), was selected for the experiments. Austenitic welding consumable Fox CN 23/12 Mo–A (wt.%: 0.01 C; 0.63 Si; 0.73 Mn; 23.0 Cr; 13.1 Ni; 2.6 Mo) was chosen for surfacing, to create an alloying gradient. Such butt joints can occur in welding boiler pipe systems, for instance, boiler manifold from R91 steel with superheaters from austenitic steels.

Two different approaches to welding were used:

1) To assess the influence of welding technique, namely angle of electrode inclination on decarburization kinetics single-pass deposits were made (to eliminate the reheating effect) on R91 steel plates, using Fox CN 23/12 Mo-A electrodes. Deposits were made at small (~30°) and large (~90°) angles of inclination. It was anticipated that each mode introduces a different degree of overheating in near-weld zone and is known to cause a reduction or increase of the dimensions of coarse-grained microstructural regions (Figure 1). A larger angle of electrode inclination promotes greater heating of the near-weld zone and contrarily — lower heating is observed at a smaller angle of inclination.

In both the cases surfacing was performed in the following mode: I_w = 120 A, U_a = 24 V, $v_w \approx$ 4.5 mm/s at room temperature.

After deposition samples were cut into two templates (Figure 2). To intensify the processes of carbon diffusion and formation of a decarburized interlayer, they were tempered at the temperature of 700 °C for 7 and 18 h. As-tempered templates were used to prepare sections, which were electrolytically etched in H_2CrO_4 for 15 s at the voltage of 10 V to reveal the decarburized interlayer.

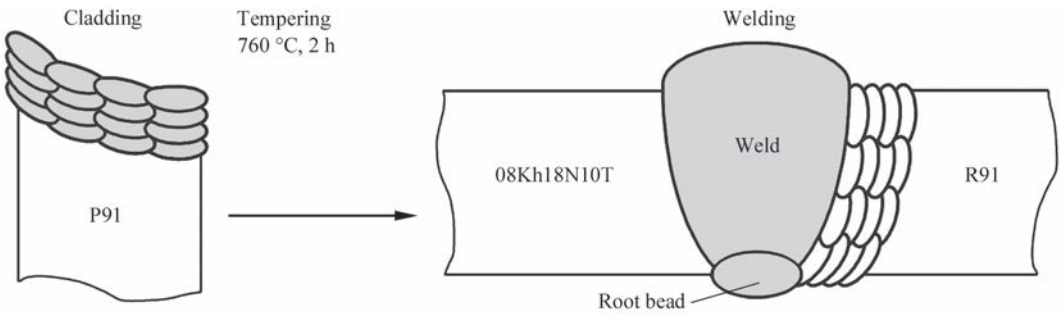

Figure 3. Scheme of cladding and welding

2) To assess the influence of the welding mode on decarburization kinetics in a real welded joint, two test joints were made on plates from martensitic steel R91 20 mm thick. Before welding the butt joints, the edges of R91 steel were first surfaced with Fox CN 23/12 Mo-A austenitic electrodes of 3.2 mm diameter in 4–5 interlayers. After surfacing the plate was tempered at 760 °C, 2 h. The surfaced and tempered edge was welded to 08Kh18N10T steel, using Fox CN 23/12 Mo-A electrodes, at current I_w = 120 A, with 60° groove angle (Figure 3). In order to ensure a high-quality formation of welded joints, root welding was performed from the reverse side of the butt after filling the groove.

The need for high-temperature tempering at the temperature of 760 °C in martensitic steel joints is attributable to the fact that dislocation excess develops in the HAZ of such steels after welding. In the presence of residual stresses, the high dislocation density accelerates the processes of recovery and recrystallization in steel that adversely affects the long-term strength [4]. High-temperature tempering leads to reduction of dislocation density and, thus, promotes an increase of long-term strength in the low loading range in high-temperature service.

Two surfacing modes were checked:

- with a small angle of inclination (~30°) at the current of I_w = 110 A;
- with a large angle of inclination (~90°) at the current of I_w = 130 A.

After welding, tempering at 700 °C for 14 h was performed for part of the samples to simulate the thermal impact in service (corresponds to ~16.8 thou h at the temperature of 600 °C at conversion using Larsen–Miller parameter [14]. After welding and tempering, sections were prepared from the samples. The microstructure of welded joint metal was revealed by electrolytic etching in chromic acid (U = 10 V, t = 10 s). Microhardness was measured in PMT-3 hardness meter at 100 g load. Metallographic analysis was performed using NEOPHOT-3 optical microscope.

In publications, for instance [15], the notion of effective width of the diffusion interlayer is used, which is determined by the shortest distance from the saturation surface (for instance, fusion line) to the measurement region. This width is characterized by established nominal values of basic parameter, which is taken to be either the diffusing element concentration, or the property (hardness) or structural feature, such as weak etchability of this region. At the same time, it is rather complicated to precisely determine the carbon content, using modern methods of elemental analysis (for instance, us-

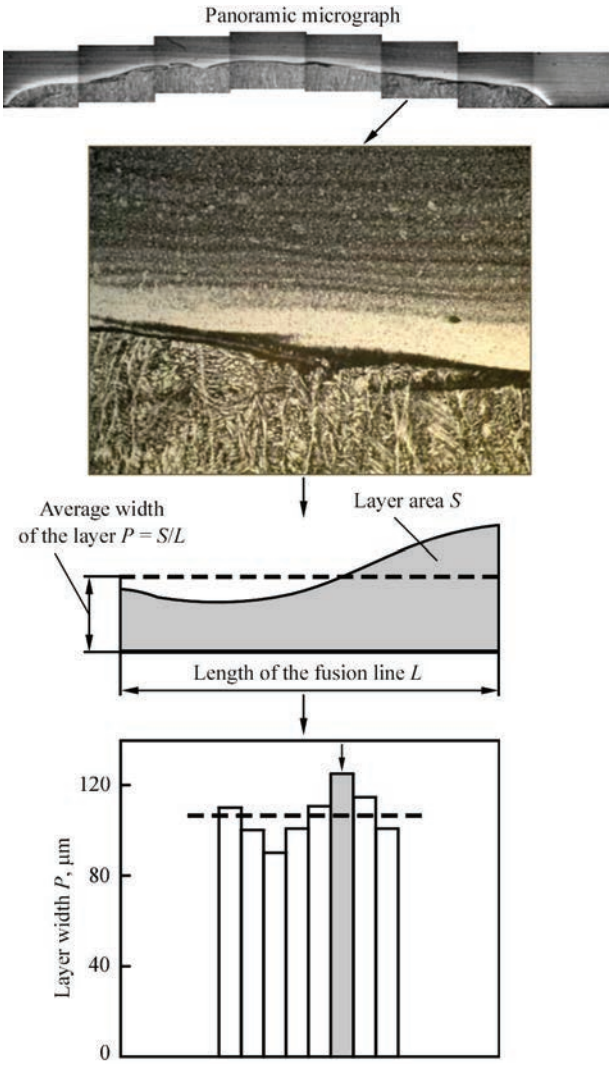

Figure 4. Scheme of plotting the histograms (adapted from [12])

ing electron probe X-Ray microanalysis), because carbon is a light element ($Z > 10$) [1].

Panoramic micrographs of the structure along the fusion line were taken at ×100 magnification, in order to determine the average width of the decarburized interlayer in the tempered deposits. From 8–9 (for deposits) to 16–17 (for welded joints) micrographs were obtained, depending on the length of the fusion line. The area of the weakly-etched near-weld zone and length of the fusion line were measured using free ImageJ software [16]. Measurement results were used to plot histograms for the case of variation of the angle of electrode inclination at surfacing and of the welding mode. Each bar of the histograms reflects the interlayer width in a certain micrograph, the bars are located in the order of filming and numbering of the micrographs from the bead left edge to its right edge (Figure 4).

Mean values of diffusion interlayer width P for each bead (dash line in the histograms) were found by the following formula

$$P = \frac{\sum_{i=1}^{n}(p_i l_i)}{\sum_{i=1}^{n} l_i},$$

where p_i is the width of the diffusion interlayer (μm) in a certain micrograph (n is the total number of micrographs for a certain bead); l_i is the length of the fusion line (μm) in a certain micrograph i.

EXPERIMENTAL RESULTS AND THEIR ANALYSIS

Figure 5 gives examples of micrographs of near-weld zone of R91 steel in the deposits after tempering at 700 °C, for 7 and 18 h, respectively, Figure 6

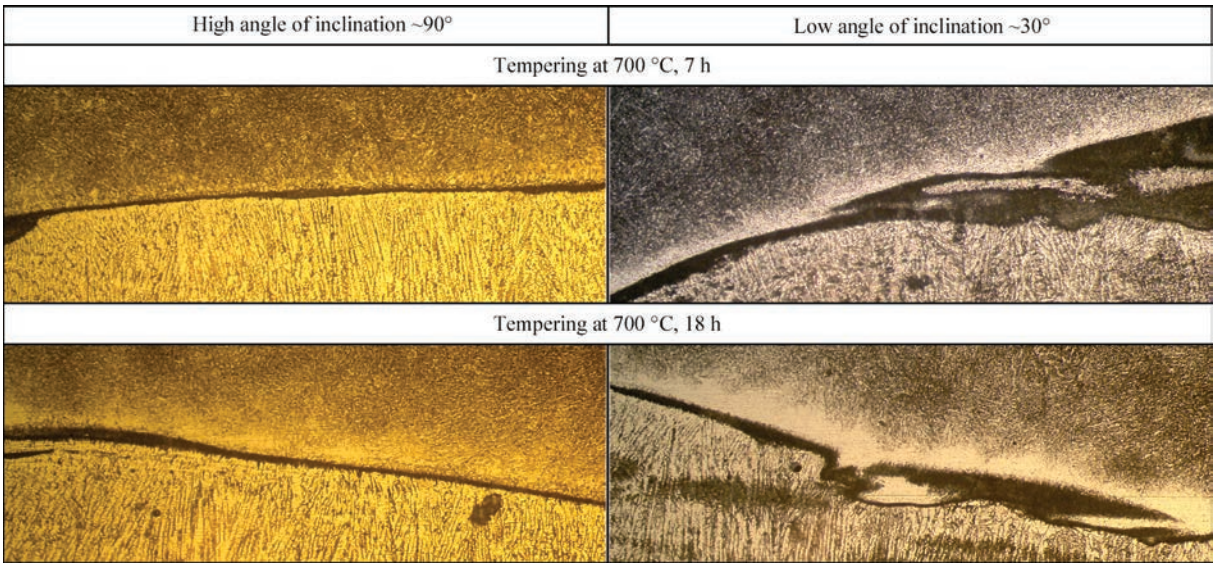

Figure 5. Example of micrographs to determine the interlayer width, depending on the angle of inclination after tempering, ×100 (lower weld)

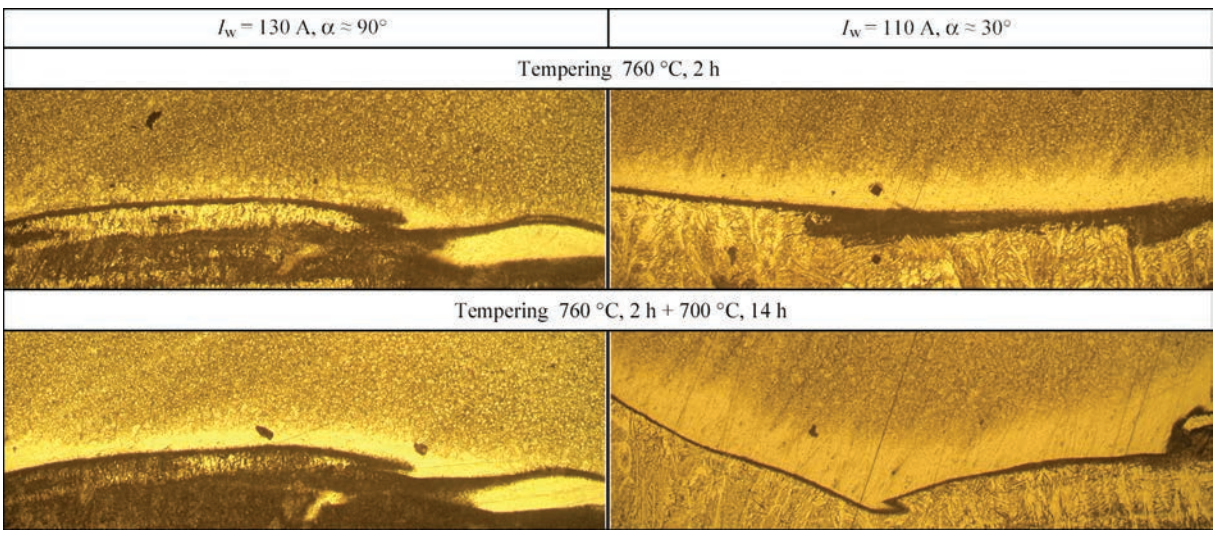

Figure 6. Example of micrographs to determine the interlayer width, depending on welding mode after tempering, ×100 (lower weld below)

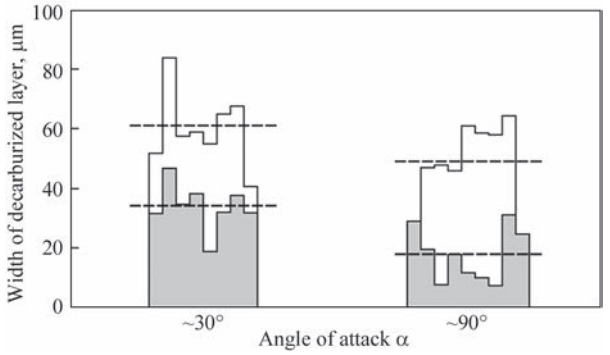

Figure 7. Histograms of the dependence of decarburized interlayer width on parameters of the angle of electrode inclination in the near-weld zone of R91 steel after tempering at 700 °C, for 7 h (contour filled with gray colour) and at 700 °C, for 18 h (contour filled with white colour)

are welded joint micrographs. A noticeable range of variation of the decarburized interlayer width at the same temperature holding can be seen in these micrographs. Figure 7 shows the built by the above procedure histograms of the decarburized interlayer width, depending on the parameter of the angle of electrode inclination after tempering at 700 °C for 7 and 18 h, and Figure 8 presents histograms of the decarburized interlayer width, depending on the surfacing mode in the welded joint after tempering at 760 °C, for 2 h and at 760 °C for 2 h + 700 °C for 14 h.

Additional measurement of microhardness in welded joints in the HAZ of R91 steel under the middle of the second clad bead from the top was performed for both the welding modes (Figure 9). The results show that in the mode with lower current and higher decarburization a noticeable softening is observed in the near-weld zone, as well as in the zone of critical temperatures between A_{C1} and A_{C3}, compared to the mode at a higher current and with lower decarburization. It enables establishing a direct relationship between the structural and mechanical characteristics of the metal, as a result of carbon diffusion in the near-weld zone:

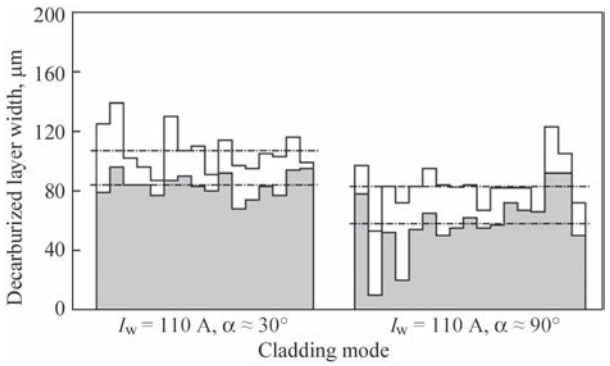

Figure 8. Histograms of the dependence of decarburized interlayer width on the parameters of welding mode in the near-weld zone of R91 steel after tempering at 760 °C for 2 h (gray coloured contour)

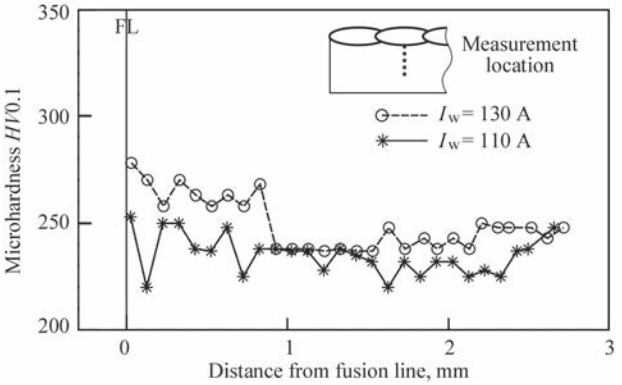

Figure 9. Microhardness in the HAZ near-weld zone of R91 steel after tempering at 760 °C, for 2 h + 700 °C, 14 h

softening becomes greater with increase of decarburization visible in the micrographs.

The data obtained from the histograms agree with investigation results, described in the previous paper [12]: the rate of development of the decarburized interlayer at tempering decreases at increase of the heat input. This is related to the fact that at the temperatures of high tempering and lower, diffusion along the grain boundaries is the prevailing type of diffusion. At surfacing at high mode parameters, the area of grain boundaries per a unit of volume becomes smaller than that in the metal with a deposit made at lower parameters, as a result of growth of primary austenite grain in the near-weld zone that limits the grain-boundary diffusion.

Grain-boundary diffusion is a complex process which includes direct diffusion through the grain lattice, diffusion along the grain boundaries, scattering of the diffusing substance from the grain boundaries and its subsequent infiltration into the grain lattice around the intergranular boundaries [17]. Different diffusion kinetics (or diffusion modes) can be observed, depending on prevalence of one of these elementary processes. Each mode prevails in a certain temperature range and soaking duration at these temperatures, and it also depends on grain dimensions, lattice parameters and grain boundaries.

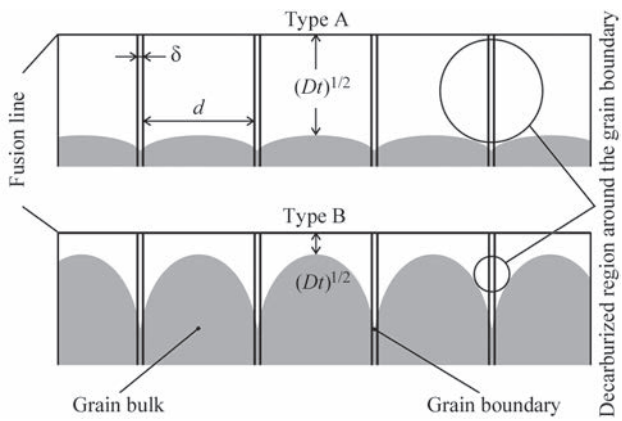

Figure 10. Diffusion kinetics of type A and B (using the data of [17])

Figure 10 shows two of the three types of diffusion kinetics classification.

KINETICS OF TYPE A

This kinetics is observed at high-temperature or long-term soaking at higher temperature in materials with small-sized grains. In work [18] it is shown that realization of such kinetics requires that the diffusion length $\sqrt{Dt}$ (where D is the coefficient of diffusion in the lattice (m^2/s); t is the time from the start of diffusion (c)) was only a little larger than the distance between the grain boundaries d:

$$\sqrt{Dt} \geq \frac{d}{0,8}.$$

In such a case, the decarburized regions around the adjacent grain boundaries overlap, and the decarburization front can capture the grain bulk.

KINETICS OF TYPE B

This kinetics is characteristic for materials after soaking at lower temperatures and/or at relatively short soaking duration in materials with sufficiently large grain size. Under such conditions, diffusion length $\sqrt{Dt}$ ahead of the grain body can become much smaller, than the distance between the grain boundaries d. At the same time, the width of near-boundary decarburized regions that is also calculated using $\sqrt{Dt}$ can be much greater than the width of grain boundaries, δ. Therefore, the following condition is satisfied for kinetics of type B:

$$\delta \ll \sqrt{Dt} \ll d.$$

At this kinetics, decarburization takes place from regions around the grain boundaries into carbon-depleted boundary regions of the grains, where diffusion has already occurred. However, unlike type A, the decarburized regions around adjacent grain boundaries do not overlap in the grain bulk [17].

At increase of grain size, type A kinetics gradually develops into type B kinetics, so that any deviations in grain size distribution in the HAZ near-weld zone after welding, caused by different heat input, will result in different decarburization rate. These data show that from the view point of the process of containment the decarburization, the coarse-grained structure has advantages over the fine-grained one. The coarse-grained structure also has a positive effect on long-term strength. This is attributable to the fact that deformation and destruction at high temperatures often take place along the grain boundaries, which have a large number of defects (vacancies, dislocations, etc.): at higher temperatures and presence of stresses elementary events of slipping and nucleation of cavities and microcracks easily occur along them, which lead to decohesion of grain boundaries [4, p. 346]. Thus, while at low temperatures the high density of grain boundaries (at fine-grained structure) promotes deceleration of dislocation motion and alloy hardening, at high temperatures, contrarily, the high density of the boundaries facilitates accelerated softening of polycrystalline metals. Therefore, coarser grain promotes an increase of high-temperature strength [15, p. 302].

The disadvantages of the coarse-grained structure in the HAZ near-weld zone are lower ductility and impact toughness, and in low-alloyed steels also the susceptibility to formation of tempering cracks. However, in the case of R91 steel, it was reported that it is not prone to temper cracking [4]. As regards impact toughness, the most critical portion of martensitic and ferritic steel joints is the region of the first cladding interlayer: intensive dilution and mixing take place in the first deposited beads with different ratios of the melt of base metal with electrode metal. In particular, nickel content in the mixed zone decreases in the direction away from the melting zone to the less alloyed base metal. In a certain point in the region of this lowering the nickel content becomes too low to stabilize austenite at cooling to room temperature, but the relatively high alloying level in this zone promotes a high hardness resulting in martensite formation there [2]. In particular, performed impact toughness testing in the first interlayer of both the deposits — at 110 and 130 A — showed that *KCV* value in this region varies within 30 J/cm^2. This zone, however, did not make any negative effect on other properties in the condition after welding and tempering — bend angle of transverse samples was not less that 100°, and fracture at static tensile testing of transverse samples occurred in the austenitic base metal.

CONCLUSIONS

1. It is established that the width of the decarburized interlayer in R91 steel, clad and welded by austenitic welding consumable, which develops at tempering or in high-temperature service, can vary at the change of values of the angle of electrode inclination: interlayer width decreases at the angle close to 90°, and increases at reduction of the angle of inclination to 30°. The width of the interlayer on samples made with angle of inclination of 30°, is greater than that on samples made with angle of inclination of 90°, after soaking at 700 °C for 7 h — 1.89 times, and after soaking for 18 h — 1.24 times.

2. Metallographic investigations and hardness measurements show that reduced decarburization and softening in the HAZ near-weld zone of marten-

sitic steel is observed after high-temperature tempering in the real welded joint of martensitic and austenitic steels, clad in the higher current mode (up to 130 A) than in the joint clad in the lower current mode (110 A). The width of the interlayer in the joints made at 110 A current with angle of inclination of 30°, is greater than that of the interlayer made at 130 A current with angle of inclination of 90°, after soaking at 760 °C for 2 h — 1.45 times; and after additional soaking at 700 °C for 14 h — 1.29 times.

REFERENCES

1. Lundin, C.D., Khan, K.K., Yang, D. (1995) Effect of carbon migration in Cr–Mo weldments on metallurgical structure and mechanical properties. *Welding Research Council Bull.*, **407**, 1–49.
2. DuPont, J.N. (2012) Microstructural evolution and high temperature failure of ferritic to austenitic dissimilar welds. *Int. Materials Reviews*, 57(**4**), 208–234.
3. Dawson, K.E., Tatlock, G.J., Chi, K., Barnard, P. (2013) Changes in precipitate distributions and the microstructural evolution of P24/P91 dissimilar metal welds during PWHT. *Metallurg. and Mater. Transact. A*, **44**, 5065–5080.
4. Abe, F., Kern, T.-U., Viswanathan, R. (2008) *Creep-resistant steels.* Cambridge, Woodhead Publishing.
5. Helander, T., Andersson, H.C.M., Oskarsson, M. (2000) Structural changes in 12–2.25 % Cr weldments — an experimental and theoretical approach. *Mater. High Temp.*, 17(**3**), 389–396.
6. Brett, S.J. (2004) Type IIIa cracking in 1/2CrMoV steam pipework systems. *Sci. and Technol. of Welding and Joining*, 9(**1**), 41–45.
7. Frei, J., Alexandrov, B.T., Rethmeier, M. (2019) Low heat input gas metal arc welding for dissimilar metal weld overlays Pt III: Hydrogen-assisted cracking susceptibility. *Welding in the World*, **63**, 591–598.
8. You, Y., Shiue, R.K., Shiue, R.H., Chen, C. (2001) The study of carbon migration in dissimilar welding of the modified 9Cr–1Mo steel. *J. of Materials Sci. Letters*, **20**, 1429–1432.
9. Karthick, K., Malarvizhi, S., Balasubramanian, V., Gourav Rao, A. (2018) Tensile properties variation across the dissimilar metal weld joint between modified 9Cr–1Mo ferritic steel and 316LN stainless steel at RT and 550 °C. *Metallography, Microstructure and Analysis*, **7**, 209–221.
10. Urzynicok, M., Jachym, R., Kwiecinski, K. et al. (2013) Application of EPRI87 in dissimilar welding austenitic martensitic welded joints of TEMPALOY AA-1 and T92 steel grades. In: *Proc. of 7th Inter. Conf. on Advances in Materials Technology for Fossil Fuel Power Plants* (*Waikoloa, Hawaii, USA)*, 992–1005.
11. Coleman, K., Gandy, D. (2007) Alternative filler materials for DMWs involving P91 materials. Advances in materials technology for fossil power plants. In: *Proc. of 5th Inter. Conf. on Advances in Materials Technology for Fossil Fuel Power Plants* (*Marco Island, Florida, USA)*, 940–967.
12. Nimko, M.O. (2021) Influence of welding parameters on decarburization in heat affected zone of dissimilar weldments after post weld heat treatment. *Archives of Materials Sci. and Engineering*, 112(**1**), 23–31.
13. Defects/imperfections in welds – reheat cracking. *Job Knowledge for Welders*, 48, TWI, July 2000, 4 p. www.twiglobal.com/technical-knowledge/job-knowledge/defectsimperfections-in-welds-reheat-cracking-048
14. Tamura, M., Abe, F., Shiba, K. et al. (2013) Larson–Miller constant of heat-resistant steel. *Metallurg. and Mater. Transact. A*, 44(**6**), 2645–2661.
15. *Lakhtin* Yu.M. (1984) *Metals science and heat treatment*. Moscow, Metallurgiya [in Russian].
16. *Image Processing and Analysis in Java*. https://imagej.nih.gov/ij/
17. Mehrer, H. (2007) *Diffusion in solids. Fundamentals, methods, materials, diffusion-controlled processes*. Springer-Verlag.
18. Belova, I.V., Murch, G.E. (2001) The transition from Harrison type-B to type-A kinetics in grain-boundary tracer diffusion. *Philosophical Magazine A*, 81(**10**), 2447–2455.

ORCID

M.O. Nimko: 0000-0002-9672-4921,
V.Yu. Skulskyi: 0000-0002-4766-5355

CONFLICT OF INTEREST

The Authors declare no conflict of interest

CORRESPONDING AUTHOR

V.Yu. Skulskyi
E.O. Paton Electric Welding Institute of the NASU
11 Kazymyr Malevych Str., 03150, Kyiv, Ukraine
E-mail: vsku@paton.kiev.ua

SUGGESTED CITATION

M.O. Nimko, V.Yu. Skulskyi, A.R. Gavryk, I.G. Osypenko (2022) Influence of welding modes on decarburization in the HAZ of R91 steel in welded joints of dissimilar steels after high-temperature tempering. *The Paton Welding J.*, **3**, 27–33.

JOURNAL HOME PAGE

https://pwj.com.ua/en

Received: 17.01.2022
Accepted: 16.05.2022